Distribution Agreement

In presenting this thesis as a partial fulfillment of the requirements for a degree from Emory University, I hereby grant to Emory University and its agents the non-exclusive license to archive, make accessible, and display my thesis in whole or in part in all forms of media, now or hereafter now, including display on the World Wide Web. I understand that I may select some access restrictions as part of the online submission of this thesis. I retain all ownership rights to the copyright of the thesis. I also retain the right to use in future works (such as articles or books) all or part of this thesis.

Hanyao Sun April 9, 2019

Numerical Simulation of Hemodynamics of Left Ventricular Assist Device for Surgical Planning

by

Hanyao Sun

Alessandro Veneziani
Adviser

Department of Mathematics and Computer Science

Alessandro Veneziani

Adviser

Manuela Manetta

Committee Member

Kate O'Toole

Committee Member

2019

Numerical Simulation of Hemodynamics of Left Ventricular Assist Device for Surgical Planning

By

Hanyao Sun

Alessandro Veneziani

Adviser

An abstract of
a thesis submitted to the Faculty of Emory College of Arts and Sciences
of Emory University in partial fulfillment
of the requirements of the degree of
Bachelor of Sciences with Honors

Department of Mathematics and Computer Science

2019

Abstract

Numerical Simulation of Hemodynamics of Left Ventricular Assist Device for Surgical Planning
By Hanyao Sun

Left ventricular assist devices (LVAD), which facilitate blood flow from the left ventricle to the aorta, are a surgical option for patients with end-stage congestive heart failure, a condition that the heart fails to pump enough blood to meet the body's need. LVAD can be surgically implanted through a left thoracotomy with outflow-graft anastomosis. Generally, the approach of LVAD should be considered when the left ventricle fails to provide more than 70% of blood flow. In this research, we investigated on three LVAD configuration positions: axial-flow and transversal-flow LVAD on ascending aorta and axial-flow LVAD on descending aorta. The position at which the graft is configured may have important clinical consequences depending on various severity of heart failure. We describe a computer-generated model to illustrate the flow dynamics in the aorta with respect to different outflow-graft configurations under various degrees of heart failure.

The simulation indicates that the location of the anastomosis has important effect on blood flow in the ascending aorta, the aortic arch and the descending aorta. Moreover, under the condition of 50% blockage of aortic root, LVAD is not generally recommended because the hazard associated with open heart surgery could outweigh its overall benefit. However, our simulation suggests that if LVAD is implanted under such condition, its configuration position does not make a significant impact to hemodynamics inside the aorta comparing to that of premorbid aorta. Under the condition of 70% blockage of aortic root, this is when LVAD implantation should be generally considered. The simulation indicates that under this scenario, axial-flow LVAD on descending aorta is the most optimal solution. The most extreme case of heart failure is 100% blockage of aortic root, meaning that the only source of blood supply is through LVAD. The simulation indicates that under this extreme case, transversal-flow LVAD on ascending aorta could be the most promising option. Results of this study provide insight on the importance of the anastomosis location on the hemodynamics in the aorta, systolic pressure on the aortic wall, velocity and vorticity of blood flow inside the aorta.

Keywords: Hemodynamics, Navier-Stokes Fluid Dynamics, LVAD, Computational Simulation, Surgical Planning

Numerical Simulation of Hemodynamics of Left Ventricular Assist Device for Surgical Planning

By

Hanyao Sun

Alessandro Veneziani

Adviser

A thesis submitted to the Faculty of Emory College of Arts and Sciences
of Emory University in partial fulfillment
of the requirements of the degree of
Bachelor of Sciences with Honors

Department of Mathematics and Computer Science

2019

Acknowledgements

My special thanks to Professor Alessandro Veneziani, my advisor, who guided me through the entire research with patience and kindness. In addition to my research partner, Imran Shah, who also put a lot of effort and dedication into this project. Last but not least, a special thanks to my other committee members, Dr. Manetta and Dr. O'Toole. This project couldn't be concluded without your support.

Table of Contents

1: Introduction

Cardiovascular diseases and the resulting deaths are the most common cause in the US fatality with approximately 610,000 deaths every year, 25% of all deaths in 2018 [8]. Congestive heart failure, which occupies a large portion of cardiovascular diseases, is a condition that the insufficient blood supply from heart fails to meet the needs of organs and tissue with oxygen and nutrients. Many causes could result in the impaired pumping efficiency of the heart. The most common ones that could lead to congestive heart failure are coronary artery disease, alcohol abuse and disorders of the heart valves.

Left ventricular assist device (LVAD) is a promising treatment for congestive heart failure. The inflow conduit of the LVAD is connected to the apex of left ventricle and the outflow conduit is connected to the aorta to enable the oxygenated blood circulation throughout the body. Figure 1 is a simplified demonstration of LVAD in relation with the left ventricle.

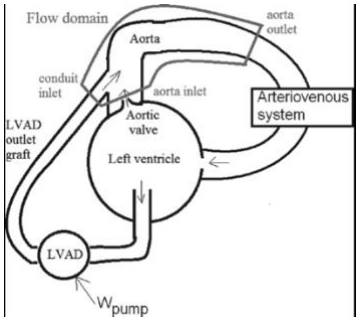

Figure 1: Simplified Demonstration of LVAD in Relation with Left Ventricle [1]

The major functions of the cardiovascular system are to distribute oxygen, nutrients and endocrine hormones throughout the body and to recycle waste products and carbon dioxide for excretion. Its functionality is closely related to the role played by aorta. It is capable of adapting

blood flow in response to different organ demands. To fulfill this function of providing sufficient blood to various tissue beds, the aortic wall has smooth muscles and high collagen and elastin content, which not only provides aorta with integrity and compliance but also regulates blood flow condition through intimal thinning or thickening.

Albeit an efficient option to treat cardiac insufficiency, the introducing of LVAD through surgical procedure could significantly disrupt a patient's premorbid aortic hemodynamics and may also lead to numerous unforeseeable post-operational complications. Many studies have been done to improve the performance of LVADs as well as to anticipate its complications. One of the studies suggest that LVAD could severely damage the hemodynamics in the left ventricle [1]. This may develop into complications such as aortic aneurysm and platelet activation, which in turn could possibly lead to stroke and further stenosis respectively. Hence, a detailed understanding of the aortic hemodynamic after implanting LVAD can have useful clinical implications in view of monitoring the short-term and long-term post-operational effect.

In the past, the adoption of mathematical modeling to study cardiovascular disease was not recommended because of the difficulties of accurately predicting the flow in specific districts of interest. Experiments back then were mostly on in vitro models or on animals. Recent technological advances in data acquisition and three-dimensional simulation, however, enable physicians to provide detailed predictions on the unforeseeable side effect of LVAD. The development of computational techniques in fluid dynamics (CFD) found a promising field of cardiovascular research. CFD could be useful in monitoring the compromised aortic hemodynamics due to LVAD and its effects on the aortic wall. A more exciting aspect of CFD is that it enables the carrying out of simulation at low costs and in controlled conditions. It also allows

physicians to examine a patient with non-invasive approach, which could significantly reduce the complications and risks associated with traditional medical approaches.

This article investigates effects of the location of the LVAD outlet graft and the percentage of blood flow the LVAD contributes to the overall blood flow by idealizing the aorta geometry as a straight cylinder and a three-dimensional arc (Figure 2 & 3):

Figure 2: Real Aorta [1]

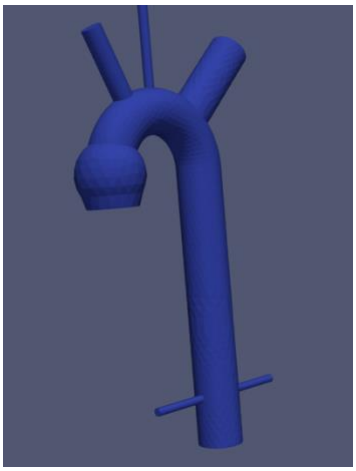

Figure 3: Idealized Aorta

Three simplified anastomosis geometries were computationally constructed with LVAD on coronal plane of ascending aorta, on transversal plane of ascending aorta and on coronal plane of descending aorta. The length and cross-sectional area of aorta were obtained from real life data to maximize the external validity of this research. For each geometry, different percent of total blood flow (50%, 70% and 100%) is prescribed to LVAD outlet graft, which corresponds to different severity of cardiovascular disease. The simulation is performed with computational fluid dynamics (CFD) of the aortic blood flow which was derived from Navier-Stokes equations.

The effect of LVAD's position and the prescribed blood flow percentage through LVAD is investigated. We examined the hemodynamics of pre-morbid aorta and aorta with LVAD in light of three various parameters that play an important role in the overall well-being of a patient's cardiovascular system: namely the systolic pressure of aorta, and the velocity and the vorticity of blood flow through aorta. The systolic pressure and the velocity of blood flow in aorta are crucial for blood distribution throughout various tissue beds. And blood vorticity is an indicator of turbulent blood flow. Generally, blood flow is laminar. However under certain conditions particularly in ascending aorta, it can be disrupted and turn into disturbed or even turbulent (Figure 4 & 5).

Figure 4: Laminar Flow [4]

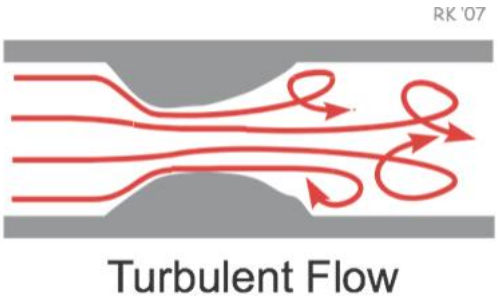

Figure 5. Turbulent Flow [4]

Even though disturbed flow may be observed in a healthy aorta, nevertheless, some research suggests that highly disturbed flow can result in postsurgical neointimal hyperplasia and may be one of the contributing factors to pathological conditions. Therefore, comparing premorbid aorta and aorta with LVAD, we took these three parameters into consideration to determine which LVAD outflow conduit position can function optimally under various extent of blockage of aortic root (50, 70 and 100%).

2. Geometric Modeling

The physiological anatomy of the aorta in a healthy human body is shown below (Figure. 6):

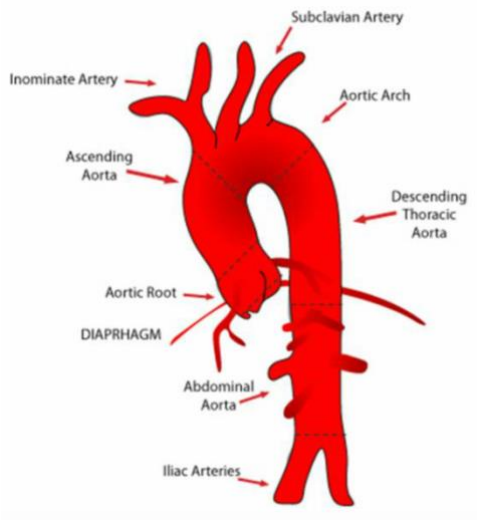

Figure 6 [3]

Three-dimensional idealized aortic geometry was constructed using Netgen (website: www.netgen.org), a computational mesh and geometry generator. The aortic root (Sinus of Valsalva) is represented in the geometry as the overlap region between two distinct spheres; the aortic arch is represented by half of a torus; the arteries that branch out of the aortic arch including brachiocephalic, carotid, subclavian arteries from left to right respectively are idealized as three straight cylinders and the descending aorta and the left and right abdominal artery are idealized as three straight cylinders as well.

The geometric parameters of the lengths of each part of the aorta and the radius of cross-sectional areas are shown in the table below based on physiological data of a healthy human individual:

Aortic part	Length (cm)
Radius of Valsalva Sinus	1.735
Cross Sectional Radius of Aortic Arch	1.375
Radius of Descending Aorta	1.375
Radius of Brachiocephalic Artery	0.6
Radius of Carotid Artery	0.29
Radius of Subclavian Artery	1.22
Radius of Left Renal Artery	0.25
Radius of Right Renal Artery	0.25
Vertical distance between Aortic Arch and Renal Artery	12

Table 1

A mesh of triangular cells is fitted via Netgen on the outer surface of the aorta and the computational analysis of velocity and pressure on the inner surface of the aorta is carried out based on this triangular surface mesh.

The common surgical procedure is to connect the left ventricular assist device (LVAD) outlet graft to the ascending aorta or descending aorta, two different approaches practiced in the US and the UK respectively. In this paper, LVAD is configured at three positions: 1. on coronal

plane of ascending aorta, 2. on transversal plane of ascending aorta and 3. on coronal plane of descending aorta (Figure 7 to 10). The LVAD outlet graft is represented as a rigid tube with a radius of 0.25 cm. The flow domain contains the LVAD, the ascending aorta, aortic arch, brachiocephalic artery, carotid artery, subclavian artery, descending aorta and left and right renal artery.

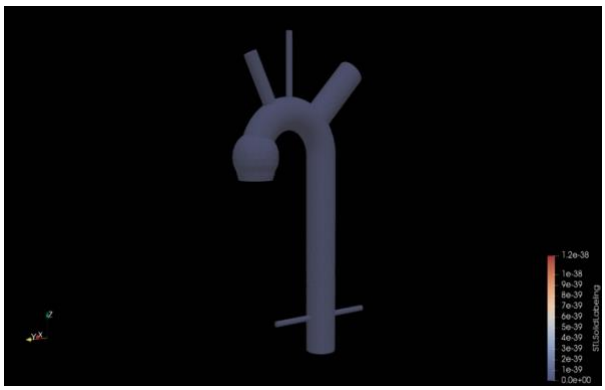

Figure 7: Control group with no LVAD

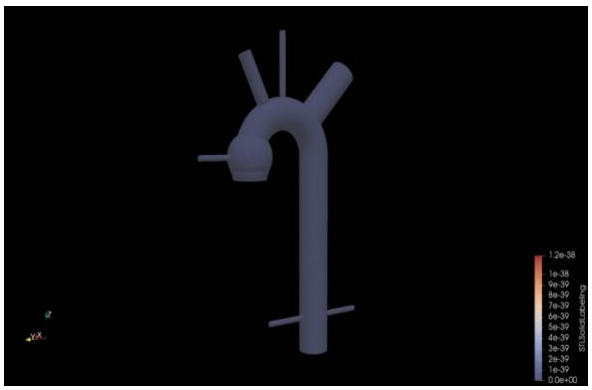

Figure 8: LVAD on Coronal Plane of Ascending Aorta

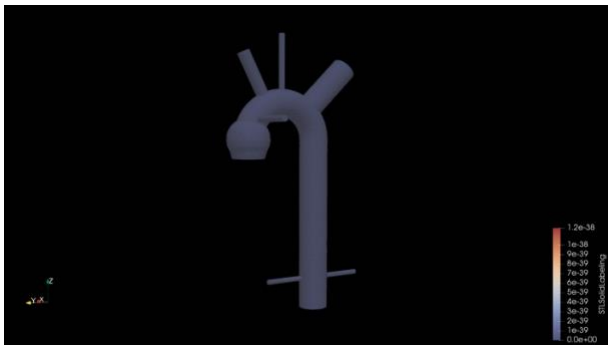

Figure 9: LVAD on Transversal Plane of Ascending Aorta

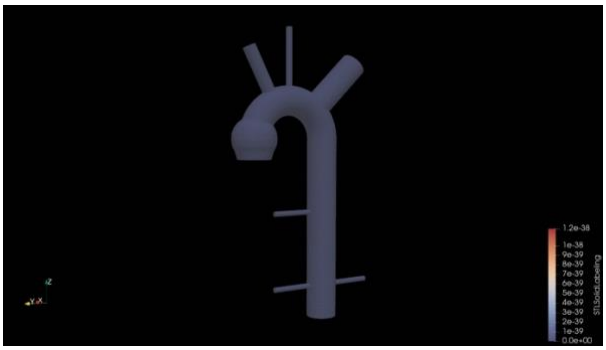

Figure 10: LVAD on Coronal Plane of Descending Aorta

3. Physical Modeling (Navier-Stokes Fluid Dynamics)

Blood is modeled as an incompressible and Newtonian fluid with the density (ρ) being 1.06 g/cm^3, the dynamic viscosity (μ) being 0.035 g/(cm · s) and the kinematic viscosity (v) being μ/ρ. Aorta and LVAD graft are modeled as rigid wall. Pulsatile flow through the aorta and LVAD is assumed.

The motion of blood in aorta is induced by the periodic contraction of the heart muscle. A heart beat consists of two phases, namely systole and diastole. During systole, the left ventricular pressure exceeds the aortic pressure, which in turn, results in a net flow from left ventricle to the aorta. During the second phase, diastole, the pressure difference is reversed resulting in the closure of aortic valve. Hence, the most prominent feature of blood flow in aorta is pulsatility, which refers to the rapid increase and decrease of blood flow rate, followed by a longer phase of the flow rate becoming small and almost constant. The total volumetric blood flow in aorta is 410 L^3 /min, which corresponds to 56 cm^3 /s and the cardiac cycle including a complete relaxation and contraction lasts approximately 0.9 seconds. Given the systolic and the diastolic condition of heart, we can represent this pulsatile flow as a simple periodic sine function with its period being 0.9 s:

$$Pulsatility = \begin{cases} 56\sin\left(\frac{\pi t}{0.3}\right) + 1 & \left(0 \le \frac{t}{0.9} \le 0.3\right) \quad (systole) \\ 1 & \left(0.3 \le \frac{t}{0.9} \le 0.9\right) \quad (diastole) \end{cases}$$

Equation Set 1

with t being time in second and the minimum flow during diastolic phase is prescribed as 1 cm^3 /s. The periodic pulsatility influences the actual velocity of blood flow in a decisive way. Given

that the morphology of the constructed geometries is relatively simple, hemodynamics inside the aorta could be obtained by coupling the geometries with Navier-Stokes fluid dynamics.

The Navier-Stokes equations are a set of partial differential equations that could be used to simulate fluid dynamics. They have their origin in applying Newton's second law to fluid motion. It also holds the assumption that the stress in the fluid is the sum of a diffusing term and a pressure term. Its application occupies a wide spectrum from magnetohydrodynamic to aerodynamics. The Navier-Stokes equations could be steady (time-independent) or unsteady (time-dependent). In this paper, since we want to examine the hemodynamics of the aorta as time elapses. The unsteady Navier-Stokes equations are a reasonable model.

3.1 Labeling Geometry

For each of the geometries, to help clarifying the boundary condition, the boundaries are labeled as following:

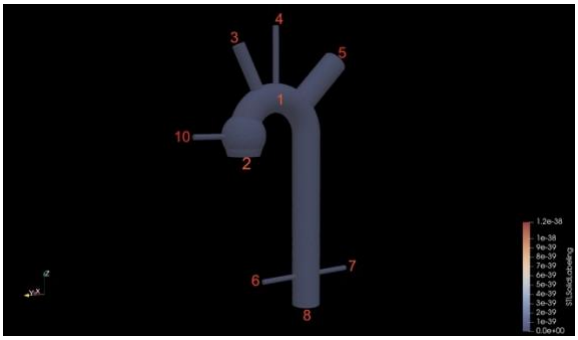

Figure 11

The entire aortic wall is labeled as 1. The LVAD outlet conduit surface is always labeled as 10 no matter what position it is configured.

We adopt the following notation: Ω is a three dimensional region denoting the portion of interest. Let $\Omega \subset \mathbb{R}^3$ be a bounded domain with boundary $\partial\Omega = \Gamma_{wall} \cup \Gamma_{out} \cup \Gamma_{in}$, such that all three parts of the boundary are mutually disjoint. Γ_{wall} include the labeled domain 1. Γ_{out} include the labeled domains 3, 4, 5, 6, 7 and 8. Γ_{in} include the labeled domains 2 and 10 (Figure 9).

3.2 Navier-Stokes Fluid Dynamics

Typical unsteady Navier-Stokes equations read:

$$\begin{cases} \dfrac{\partial u}{\partial t} + (u \cdot \nabla)u - v\Delta u + \nabla p = 0 & in \quad Q_T = \Omega \\ \nabla \cdot u = 0 & in \quad Q_T \end{cases}$$

Equation Set 2

with u being the velocity, v being the kinematic viscosity. Based on the very geometries we construct and physiological conditions, the boundary conditions for Naiver-Stokes equations are:

1. Velocity condition corresponds to 120 mmHg, normal aortic pressure: $u = 0 \; on \; \Gamma_{wall}$.
2. Resistance conditions:

$$\begin{cases} Ru \cdot n_{\partial\Omega} + n_{\partial\Omega}^T (2vD(u) - pI) n_{\partial\Omega} = 0 & on \quad \Gamma_{out} \\ 10000n = 0 & on \quad \Gamma_{out} \end{cases}$$

Equation Set 3

with D(u) being the velocity deformation tensor:

$$D(u) = \frac{\nabla u + \nabla u^T}{2}.$$

Equation 1

The unit tensor is denoted by I and α is the penetration parameter. α varies with respect to different Γ_{wall} surfaces. It assumes the values of 1, 5, 1, 5, 5 and 0 on surface 3~8 respectively.

To solve this Navier-Stokes system with boundary conditions, we can adopt the finite element method, which we use Finite Differentiation for the time discretization. We assume a uniform time step Δt. With usual notation, strong formulation of the problem discretized in time with the Implicit Euler method reads: for any $n \geq 0$, find u^{n+1} and p^{n+1} solving in Ω. $\frac{\partial u}{\partial t}$ could be represented as an approximation of:

$$\frac{\partial u}{\partial t} \approx \frac{u^{n+1} - u^n}{\Delta t}$$

Equation 2

And Equation set 2 could be rewritten as:

$$\begin{cases} \frac{u^{n+1} - u^n}{\Delta t} + (u^{n+1} \cdot \nabla) u^{n+1} - v\Delta u^{n+1} + \nabla p^{n+1} = 0 \\ \nabla \cdot u^{n+1} = 0 \end{cases}$$

Equation Set 4

However, we may notice that Equation Set 5 is not linear due to the presence of the first u^{n+1} in $(u^{n+1} \cdot \nabla) u^{n+1}$. To fix this problem without altering Navier-Stokes Equations, we could adopt the following approach. Since implicit Euler has a discretization error $O(\Delta t)$ and $u^{n+1} = u^n + O(\Delta t)$, the following discretization scheme has order 1 with a linear system to solve at each time step:

$$\begin{cases} \dfrac{u^{n+1} - u^n}{\Delta t} + (u^n \cdot \nabla)u^{n+1} - v\Delta u^{n+1} + \nabla p^{n+1} = 0 \\ \nabla \cdot u^{n+1} = 0 \end{cases}$$

Equation Set 5

3.2.1 The Weak Formulation with Pressure Condition

To represent Naiver-Stokes equations with boundary conditions on Freefem, we have to find the weak formulation of Equation Set 6. To derive the weak formulation, we set:

1. $V \equiv H_0^1(\Omega)$
2. $Q \equiv L_0^2(\Omega) = \{q \in L^2(\Omega): \int_\Omega q d\Omega = 0\}$. Given a pressure field $\tilde{p}$, pressure $p = \tilde{p} - \int_\Omega \tilde{p} d\Omega$ belongs to Q.

We then can proceed by multiplying both sides of the first equation of Equation Set 5 by a test function v integrating over Ω and using integrating by parts. After the space discretization of Equation Set 5, we get: for any n ≥ 0 find $u_h^{n+1} \in V_h$ and $p_h^{n+1} \in Q_h$ such that for any $\mathrm{v}_h \in V_h$ and $q_h \in Q_h$, we obtain:

$$\begin{cases} \dfrac{1}{\Delta t}(u_h^{n+1}, \mathrm{v}_h) + a(u_h^{n+1}, \mathrm{v}_h) + c(u_h^n, u_h^{n+1}, \mathrm{v}_h) + b(\mathrm{v}_h, p_h^{n+1}) + g(\mathrm{v}_h, p_h^{n+1}) = \dfrac{1}{\Delta t}(u_h^n, \mathrm{v}_h) \\ b(u_h^{n+1}, q_h) = 0 \end{cases}$$

Equation Set 6

where:

$$(u, \mathrm{v}) = \int_\Omega u \cdot \mathrm{v}\, d\,\Omega$$

$$a(u, \mathrm{v}) = v(\nabla u, \nabla \mathrm{v})$$

$$b(\mathrm{v}, \mathrm{p}) = -((\nabla \cdot \mathrm{v}), \mathrm{p})$$

$$c(u, \mathrm{v}, \mathrm{w}) = ((u\cdot\nabla)\mathrm{v}, \mathrm{w})$$

$$g(\mathrm{v}, \mathrm{p}) = \int_{\Gamma_{out}} 10000\mathrm{n}\cdot\mathrm{v}d\gamma$$

Hence, by combining both equations in Equation Set 8, we can now obtain a weak formulation that includes both unsteady Navier-Stokes equations and pressure boundary conditions:

$$\frac{1}{\Delta t}(u_h^{n+1}, \mathrm{v}_h) - \frac{1}{\Delta t}(u_h^n, \mathrm{v}_h) + a(u_h^{n+1}, \mathrm{v}_h) + c(u_h^n, u_h^{n+1}, \mathrm{v}_h) + b(\mathrm{v}_h, p_h^{n+1}) + g(\mathrm{v}_h, p_h^{n+1}) + b(u_h^{n+1}, q_h) = 0$$

Equation 3

3.2.2 Integrating Resistance Conditions to Weak Formulation

After dealing with the pressure conditions, we can now integrate the resistance conditions at each outlet into the weak formulation. First we should obtain the weak formulation of the resistance condition from Equation Set 4:

$$\int_{\Gamma_{out}} (2vD(u) - pI)n_{\partial\Omega}\cdot\mathrm{v}ds$$

A few observations about this integration: $n_{\partial\Omega}$ is a unit vector and $\mathrm{v} = (\mathrm{v}\cdot n_{\partial\Omega})n_{\partial\Omega}$ because v and $n_{\partial\Omega}$ are parallel. Also since $D(u) = \frac{\nabla\mathrm{u} + \nabla u^T}{2}$ (Eq. 1)and I is an identity matrix, $(2vD(u) - pI)$ is symmetrical. Based on $\mathrm{R}u\cdot n_{\partial\Omega} + n_{\partial\Omega}^T(2vD(u) - pI)n_{\partial\Omega} = 0$, it follows that:

$$\int_{\Gamma_{out}} (2vD(u) - pI)n_{\partial\Omega}\cdot\mathrm{v}ds$$

$$= \int_{\Gamma_{out}} n_{\partial\Omega}{}^T(2vD(u) - pI)n_{\partial\Omega}(\mathrm{v}\cdot n_{\partial\Omega})ds$$

$$= -\int_{\Gamma_{out}} \mathrm{R}(\mathrm{u}\cdot n_{\partial\Omega})(\mathrm{v}\cdot n_{\partial\Omega})ds$$

$$= -\int_{\Gamma_{out}} \mathrm{R}(u_h^{n+1} \cdot n_{\partial\Omega})(\mathrm{v}_h \cdot n_{\partial\Omega}) ds$$

Equation 4

Here, we can use $r(u^{n+1}, v)$ to denote -$\int_{\Gamma_{out}} \mathrm{R}(u^{n+1} \cdot n_{\partial\Omega})(\mathrm{v} \cdot n_{\partial\Omega}) ds$. After integrating the resistance conditions into Eq. 3, the new weak formulation reads:

$$\frac{\mathbf{1}}{\Delta \boldsymbol{t}}(\boldsymbol{u}_h^{n+1}, \mathbf{v}_h) - \frac{\mathbf{1}}{\Delta \boldsymbol{t}}(\boldsymbol{u}_h^{n}, \mathbf{v}_h) + \boldsymbol{a}(\boldsymbol{u}_h^{n+1}, \mathbf{v}_h) + \boldsymbol{c}(\boldsymbol{u}_h^{n}, \boldsymbol{u}_h^{n+1}, \mathbf{v}_h) + \boldsymbol{b}(\mathbf{v}_h, \boldsymbol{p}_h^{n+1}) + \boldsymbol{g}(\mathbf{v}_h, \boldsymbol{p}_h^{n+1}) + \boldsymbol{b}(\boldsymbol{u}_h^{n+1}, \boldsymbol{q}_h) + \boldsymbol{r}(\boldsymbol{u}^{n+1}, \boldsymbol{v}) = \mathbf{0}$$

Equation 5

3.2.3 Integrating Streamline Diffusion into Weak Formulation

Numerical simulation of fluids often suffer from instabilities that require a specific treatment. Specifically, we opted for the so-called streamline diffusion that we illustrate hereafter. In general, the streamline diffusion term reads: $u(u \cdot D\nabla^2 u)$. This has, in fact, a stabilizing effect. Again, we have to obtain its weak formulation in order to integrate it into Eq. 6. We can denote the streamline diffusion as $sd(u_h^n, \mathrm{v}_h, u)$:

$$sd(u_h^n, \mathrm{v}_h, u) = \mathrm{D}(\nabla u^n \cdot u, \nabla v_h \cdot u) .$$

Now, we have the complete weak formulation:

$$\frac{\mathbf{1}}{\Delta \boldsymbol{t}}(\boldsymbol{u}_h^{n+1}, \mathbf{v}_h) - \frac{\mathbf{1}}{\Delta \boldsymbol{t}}(\boldsymbol{u}_h^{n}, \mathbf{v}_h) + \boldsymbol{a}(\boldsymbol{u}_h^{n+1}, \mathbf{v}_h) + \boldsymbol{c}(\boldsymbol{u}_h^{n}, \boldsymbol{u}_h^{n+1}, \mathbf{v}_h) + \boldsymbol{b}(\mathbf{v}_h, \boldsymbol{p}_h^{n+1}) + \boldsymbol{g}(\mathbf{v}_h, \boldsymbol{p}_h^{n+1}) + \boldsymbol{b}(\boldsymbol{u}_h^{n+1}, \boldsymbol{q}_h) + \boldsymbol{r}(\boldsymbol{u}^{n+1}, \boldsymbol{v}) + \boldsymbol{sd}(\boldsymbol{u}_h^{n}, \mathbf{v}_h, \boldsymbol{u}) = \mathbf{0}$$

Equation 6

4: Code

Code for the computer-based geometries:

```
#
##
#
algebraic3d

solid valsalva_sinus_ball = sphere (0, 7, 0.86; 1.735)
       and plane ( 0, 7, 0; 0, 0, -1);
#      and plane ( 0, 7, 1.828; 0, 0, 1);

solid supra_coronary_aneurysm = sphere (0, 7, 1.8375; 2.05)
       and plane ( 0, 7, 0.5; 0, 0, -1);
#      and plane ( 0, 7, 1.828; 0, 0, 1);

solid valsalva_sinus = valsalva_sinus_ball or supra_coronary_aneurysm;

solid ascending = torus ( 0, 3.5, 1.8375; 1, 0, 0; 3.5; 1.375 )
       and plane ( 0, 7, 1.8375; 0, 0, -1);

solid descending = cylinder ( 0, 0, 2; 0, 0, -16; 1.375 )
    and plane (0, 0, 1.8375; 0, 0, 1)
    and plane (0, 0, -15; 0, 0, -1);

solid top_graft = cylinder(0, 6.5, 3.7; -18, 6.5,3.7; 0.29)
    and plane(0, 6.5, 3.7; 1, 0, 0)
    and plane(-6, 6.5, 3.7;-1, 0, 0);

solid brach_trunk = cylinder(0, 4.5, 4; 0, 7.5, 10; 0.6)
    and plane(0, 4.5, 4; 0, -1, -1)
    and plane(0, 7.5, 10; 0, 1, 2);

solid left_carotid_artery = cylinder(0, 3.5, 3.5; 0, 3.5, 18; 0.29)
    and plane(0, 3.5, 6; 0, 0, -1)
    and plane(0, 3.5, 12; 0, 0, 1);

solid left_subclavian_artery = cylinder(0, 1.5, 4; 0, -3.5, 9; 1.22)
    and plane(0, 1.5, 4; 0, 1, -1)
    and plane(0, -3.5, 9; 0, -1, 1);

solid right_renal_artery = cylinder(0, 0, -12; 0, 5, -12; 0.25)
    and plane(0, 0, -12; 0, -1, 0)
    and plane(0, 5, -12; 0, 1, 0);

solid left_renal_artery = cylinder(0, 0, -12; 0, -5, -12; 0.25)
    and plane(0, 0, -12; 0, 1, 0)
    and plane(0, -5, -12; 0, -1, 0);


solid arch = valsalva_sinus or ascending or left_carotid_artery or left_subclavian_arte
ry or top_graft or brach_trunk;

solid aorta = arch or descending or right_renal_artery or left_renal_artery;

tlo aorta;
```

Code for Navier-Stokes equations: With the weak formulation, we can use Freefem to computationally solve for the velocity and pressure with respect to time. The Freefem code reads:

```
1.  //Unsteady Stokes problem for a TCPC
2.  // UNITS
3.  // grams, seconds, centimeters
4.  load "msh3"
5.  //load "iovtk"
6.  load "medit"
7.  load "gmsh"
8.  string path="./";
9.  mesh3 Th = gmshload3(path+"aorta_valsalva_bav_lateral_fine.msh"); // Load the geometrie
    s
10. verbosity = 1;
11. real rho = 1.06; // Density (g/cm^3)
12. real mu = 0.035; // Dynamic viscosity (g/cm.s)
13. real nu = mu/rho; // Kinematic viscosity
14.
15. fespace Uh(Th,P1b3d);
16. fespace Ph(Th,P13d);
17. fespace All(Th,[P1b3d,P1b3d,P1b3d,P13d]);
18. All [ux,uy,uz,p],[vx,vy,vz,q], [uxlast,uylast,uzlast,plast], [uxst,uyst,uzst,pst];
19.
20. real upm, velNorm, delta=1.; // quantities relevant for SD stabilization
21. real vsq = 2; // a very small quantity to guarantee minimal stabilization SD
22.
23. real[int] R1=[1.0, 5.0, 1.0, 5.0, 5.0, 0.0]; // Resistances of the 6 outlets
24. real[int] op=[10.e4,10.e4,10.e4,10.e4,10.e4,10.e4]; // Pressure of the 6 outlets
25.
26. macro Div(ux,uy,uz) (dx(ux)+dy(uy)+dz(uz)) //Construct a function for divergence
27. macro Grad(u) [dx(u), dy(u), dz(u)] // Construct a vector for gradient
28. macro Mass(u1, u2, u3) [u1, u2, u3]// Construct a vector for u
29. macro NL(b1,b2,b3,u) (b1*dx(u)+ b2*dy(u)+ b3*dz(u)) // Construct a function for c( 〖u_h
    ^n,u〗_h^(n+1),"v" _h )
30. load "UMFPACK64"
31.
32.
33.
34.
35. // Steady Navier Stokes (time independent)
36. problem steadyStokes([ux,uy,uz,p],[vx,vy,vz,q],solver=sparsesolver) =
37.   int3d(Th) ( nu * (Grad(ux)'*Grad(vx)+Grad(uy)'*Grad(vy)+Grad(uz)'*Grad(vz)) // a(u,v)

38. - q*Div(ux,uy,uz)+ p*Div(vx,vy,vz)) //b(v,p) and b(u,q)
39. //pressure conditions g(v, p)
40.     + int2d(Th,3)(op(0)*(vx*N.x+vy*N.y+vz*N.z))
41.     + int2d(Th,4)(op(1)*(vx*N.x+vy*N.y+vz*N.z))
42.     + int2d(Th,5)(op(2)*(vx*N.x+vy*N.y+vz*N.z))
43.     + int2d(Th,6)(op(3)*(vx*N.x+vy*N.y+vz*N.z))
44.     + int2d(Th,7)(op(4)*(vx*N.x+vy*N.y+vz*N.z))
45.     + int2d(Th,8)(op(5)*(vx*N.x+vy*N.y+vz*N.z))
46. //resistances conditions r(u,v)
47.     + int2d(Th,3)(R1(0)*(ux*N.x+uy*N.y+uz*N.z)*(vx*N.x+vy*N.y+vz*N.z))
48.     + int2d(Th,4)(R1(1)*(ux*N.x+uy*N.y+uz*N.z)*(vx*N.x+vy*N.y+vz*N.z))
49.     + int2d(Th,5)(R1(2)*(ux*N.x+uy*N.y+uz*N.z)*(vx*N.x+vy*N.y+vz*N.z))
```

```
    + int2d(Th,6)(R1(3)*(ux*N.x+uy*N.y+uz*N.z)*(vx*N.x+vy*N.y+vz*N.z))
    + int2d(Th,7)(R1(4)*(ux*N.x+uy*N.y+uz*N.z)*(vx*N.x+vy*N.y+vz*N.z))
    + int2d(Th,8)(R1(5)*(ux*N.x+uy*N.y+uz*N.z)*(vx*N.x+vy*N.y+vz*N.z))
//the dirichlet condition for the inflow
+ on(10,ux=0.0,uy=-20,uz=0.0) // inflow on surface 10
+ on(2,ux=0.0,uy=0.0,uz=40) // inflow on surface 2
+ on(1,ux=0.0,uy=0.0,uz=0.0); // zero pressure on aortic wall

cout << "Initializing with Stokes... " << endl;
steadyStokes;
cout << "done!" << endl;
  string namefilest = "LVADST" + ".vtk";
    ofstream kout(namefilest);
    include "vtkexportP1bP1.edp";
    velNorm = int3d(Th)((ux)^2 + (uy)^2 + (uz)^2);
    velNorm = sqrt(abs(velNorm));
    upm = velNorm + vsq;

[uxst,uyst,uzst,pst]=[ux,uy,uz,p];



// UNSTEADY PART
real dt=0.01; //time step
real dti=1./dt;
int nmax=200;  //number of loops


// Function for pulsatility (Eq. Set 1)
func real pulsatility(real t){
real tfr = 56.0; // corresponds to a volumetric flow rate of 410 cm^3/s as for Oluffsen and Peskin
real tp = t - floor(t/0.9)*0.9;
if (tp <= 0.3){
    return tfr * sin(pi * tp / 0.300) + 1;
}else{
    return 1;
}
}
real t=0.0;
real fract=0; // fraction of the aortic valve that is open. For each geometry examined, this number assumes 0, 0.3 or 0.5

problem unsteadyNS([ux,uy,uz,p],[vx,vy,vz,q], solver=sparsesolver) = //,solver=GMRES,eps=1.e-6) =
  int3d(Th)(dti*Mass(ux,uy,uz)'*Mass(vx,vy,vz) + // (1/Δt)(u_h^{n+1}, v_h)
   nu * (Grad(ux)'*Grad(vx)+Grad(uy)'*Grad(vy)+Grad(uz)'*Grad(vz)) // a(u_h^{n+1}, v_h)
- q*Div(ux,uy,uz) // b(u_h^{n+1}, q_h)
+ p*Div(vx,vy,vz) // b(v_h, p_h^{n+1})
+ [NL(uxlast,uylast,uzlast,ux),
     NL(uxlast,uylast,uzlast,uy),NL(uxlast,uylast,uzlast,uz)]'*[vx,vy,vz])
//c(u_h^n, u_h^{n+1}, v_h)
//pressure conditions g(v_h, p_h^{n+1}) on surface 3~8
          + int2d(Th,3)(op(0)*(vx*N.x+vy*N.y+vz*N.z))
          + int2d(Th,4)(op(1)*(vx*N.x+vy*N.y+vz*N.z))
          + int2d(Th,5)(op(2)*(vx*N.x+vy*N.y+vz*N.z))
          + int2d(Th,6)(op(3)*(vx*N.x+vy*N.y+vz*N.z))
          + int2d(Th,7)(op(4)*(vx*N.x+vy*N.y+vz*N.z))
          + int2d(Th,8)(op(5)*(vx*N.x+vy*N.y+vz*N.z))
      //resistances conditions r(u^{n+1}, v) on surface 3~8
```

```
            + int2d(Th,3)(R1(0)*(ux*N.x+uy*N.y+uz*N.z)*(vx*N.x+vy*N.y+vz*N.z))
            + int2d(Th,4)(R1(1)*(ux*N.x+uy*N.y+uz*N.z)*(vx*N.x+vy*N.y+vz*N.z))
            + int2d(Th,5)(R1(2)*(ux*N.x+uy*N.y+uz*N.z)*(vx*N.x+vy*N.y+vz*N.z))
            + int2d(Th,6)(R1(3)*(ux*N.x+uy*N.y+uz*N.z)*(vx*N.x+vy*N.y+vz*N.z))
            + int2d(Th,7)(R1(4)*(ux*N.x+uy*N.y+uz*N.z)*(vx*N.x+vy*N.y+vz*N.z))
            + int2d(Th,8)(R1(5)*(ux*N.x+uy*N.y+uz*N.z)*(vx*N.x+vy*N.y+vz*N.z))
        // Streamline diffusion sd(u_h^n, v_h, u)
        + int3d(Th)(delta/upm*hTriangle*uxlast*dx(ux)*uxlast*dx(vx)+   // streamline dif
    fusion: next 27 terms
                        delta/upm*hTriangle*uxlast*dx(uy)*uxlast*dx(vy)+
                        delta/upm*hTriangle*uxlast*dx(uz)*uxlast*dx(vz)+
                        delta/upm*hTriangle*uxlast*dx(ux)*uylast*dy(vx)+
                        delta/upm*hTriangle*uxlast*dx(ux)*uzlast*dz(vx)+
                        delta/upm*hTriangle*uxlast*dx(uy)*uylast*dy(vy)+
                        delta/upm*hTriangle*uxlast*dx(uy)*uzlast*dz(vy)+
                        delta/upm*hTriangle*uxlast*dx(uz)*uylast*dy(vz)+
                        delta/upm*hTriangle*uxlast*dx(uz)*uzlast*dz(vz)+
                        delta/upm*hTriangle*uylast*dy(ux)*uxlast*dx(vx)+
                        delta/upm*hTriangle*uylast*dy(uy)*uxlast*dx(vy)+
                        delta/upm*hTriangle*uylast*dy(uz)*uxlast*dx(vz)+
                        delta/upm*hTriangle*uylast*dy(ux)*uylast*dy(vx)+
                        delta/upm*hTriangle*uylast*dy(ux)*uzlast*dz(vx)+
                        delta/upm*hTriangle*uylast*dy(uy)*uylast*dy(vy)+
                        delta/upm*hTriangle*uylast*dy(uy)*uzlast*dz(vy)+
                        delta/upm*hTriangle*uylast*dy(uz)*uylast*dy(vz)+
                        delta/upm*hTriangle*uylast*dy(uz)*uzlast*dz(vz)+
                        delta/upm*hTriangle*uzlast*dz(ux)*uxlast*dx(vx)+
                        delta/upm*hTriangle*uzlast*dz(uy)*uxlast*dx(vy)+
                        delta/upm*hTriangle*uzlast*dz(uz)*uxlast*dx(vz)+
                        delta/upm*hTriangle*uzlast*dz(ux)*uylast*dy(vx)+
                        delta/upm*hTriangle*uzlast*dz(ux)*uzlast*dz(vx)+
                        delta/upm*hTriangle*uzlast*dz(uy)*uylast*dy(vy)+
                        delta/upm*hTriangle*uzlast*dz(uy)*uzlast*dz(vy)+
                        delta/upm*hTriangle*uzlast*dz(uz)*uylast*dy(vz)+
                        delta/upm*hTriangle*uzlast*dz(uz)*uzlast*dz(vz))
        //the dirichlet condition for the inflow
        + on(10,ux=0.0,uy=-(1-
    fract)*pulsatility(t),uz=0.0) // Flow with pulsatility on surface 10
        + on(2,ux=0.0,uy=0.0,uz=fract*pulsatility(t)) // Flow with pulsatility on surfac
    e2
        + on(1,ux=0.0,uy=0.0,uz=0.0);

        [uxlast,uylast,uzlast,plast]=[ux,uy,uz,p]; // Update the loop
        for (int i = 0; i< nmax; i++) {
            t=dt*i;
            cout<<t<< " " << pulsatility(t)<<endl;
            unsteadyNS
            [uxlast,uylast,uzlast,plast]=[ux,uy,uz,p];
        velNorm = int3d(Th)(abs((ux)^2 + (uy)^2 + (uz)^2));
        velNorm = sqrt(abs(velNorm)); //
            upm = velNorm + vsq; // Monitor the stability of the solver for each loop
           if (i % 10 == 0 && i <= nmax) {
            string namefile = "LVAD" + i + ".vtk"; // Save the results every 10 loops
            ofstream kout(namefile);
            include "vtkexportP1bP1.edp";
            }
        }
         plot(p);
            plot([ux,uy,uz]);
```

5: Computer Simulation Results

5.1: Low LVAD Output (50%)

5.1.1: Systolic Pressure in Aorta

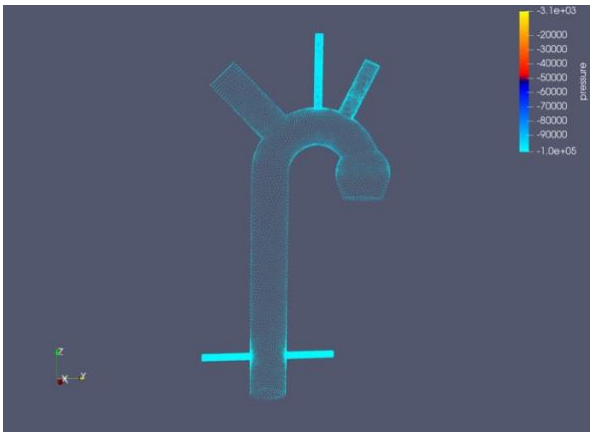

Figure 12: Pressure: Control Group

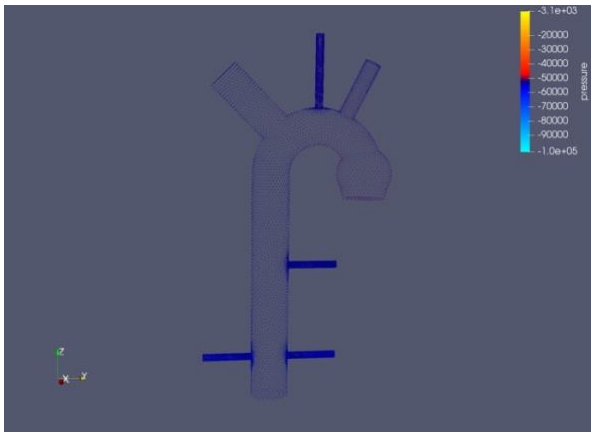

Figure 13: Pressure: Axial-Flow LVAD on Descending Aorta with Low LVAD Output

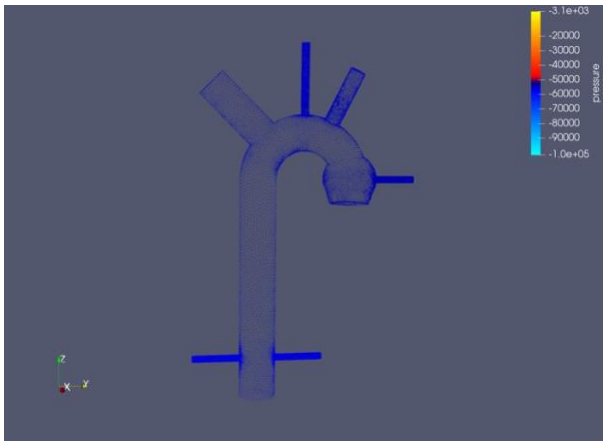

Figure 14: Pressure: Axial-Flow LVAD on Ascending Aorta with Low LVAD Output

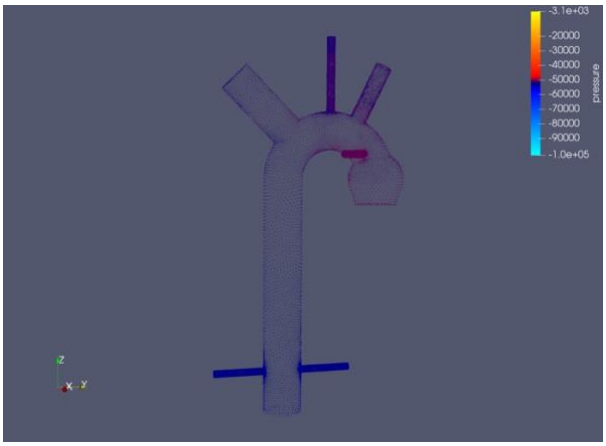

Figure 15: Pressure: Transversal-Flow LVAD on Ascending Aorta with Low LVAD Output

Since pressure is a scalar function, we can only visualize its effect on the aortic wall. Figure 12 to 15 suggest that the aortic pressure has its physiological value in the control group and LVAD

compromises this pressure to some extent, but the influence of LVAD to aortic pressure under low LVAD output is independent of outflow-graft anastomosis location.

5.1.2 The Velocity of Blood Flow

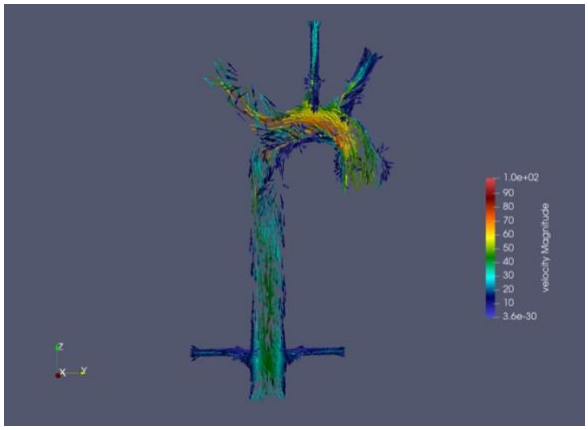

Figure 16: Velocity: Control Group

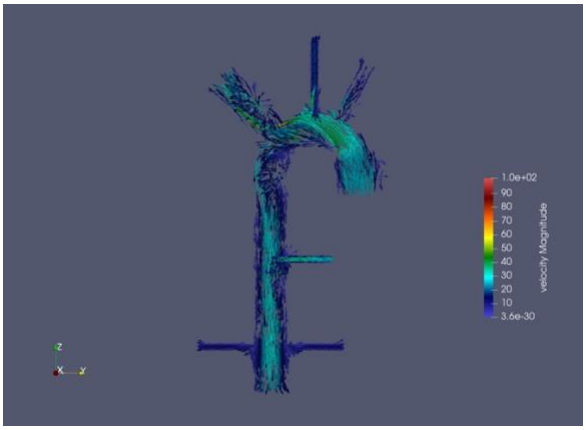

Figure 17: Velocity: Axial-Flow LVAD on Descending Aorta with Low LVAD Output

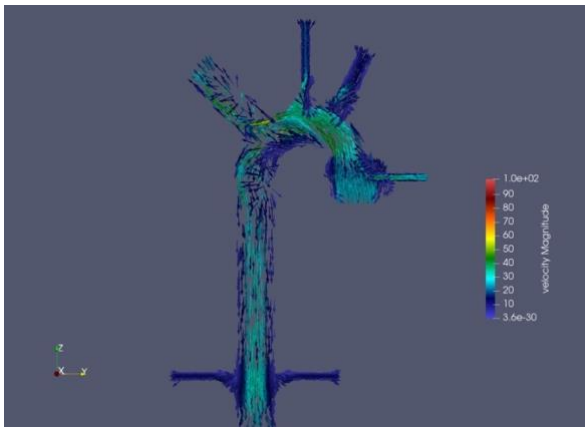

Figure 18: Velocity: Axial-Flow LVAD on Ascending Aorta with Low LVAD Output

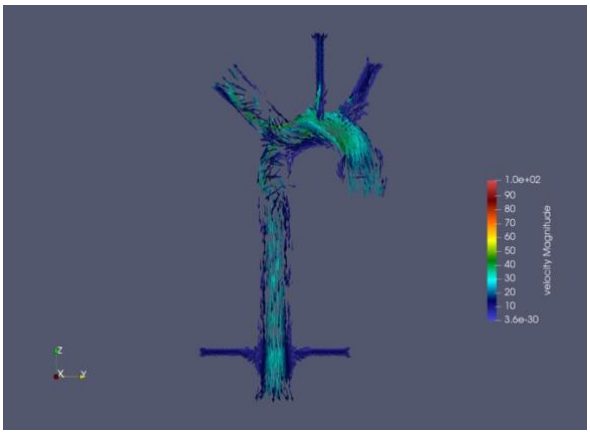

Figure 19: Velocity: Transversal-Flow LVAD on Ascending Aorta with Low LVAD Output

With the help of Paraview, an open-source multiple-platform application for interactive, scientific visualization, we are able to visualize the velocity vector field of blood flow in the cross-sectional area. Under low LVAD output condition, the control group has the highest velocity in the aortic arch area and the total blood flow from aorta could be distributed evenly to the outflow

surfaces, which include brachiocephalic, carotid, subclavian, renal artery and descending aorta. Likewise, the hemodynamics of the aorta with LVAD shows similar pattern of velocity gradient throughout the entire aorta and the total blood flow provided by LVAD and native aortic root is sufficient to supply the outflow arteries. Even though the velocities of blood inside the aortic arch with LVAD are lower than the control group in aortic arch, they themselves show little to no difference in terms of velocity. Therefore, since the blood could be supplied evenly to the output arteries, the location of anastomosis does not make a significant difference.

5.1.3: Vorticity

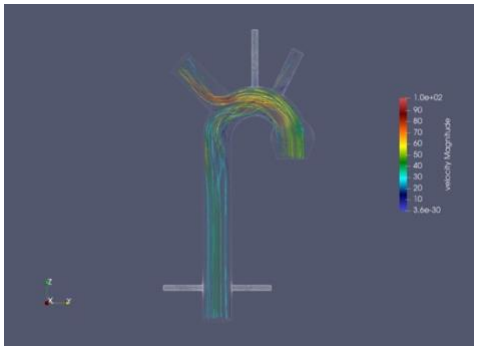

Figure 20: Vorticity: Control Group

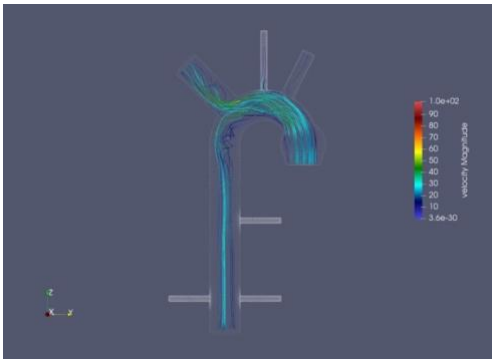

Figure 21: Vorticity: Axial-Flow LVAD on Descending Aorta with Low LVAD Output

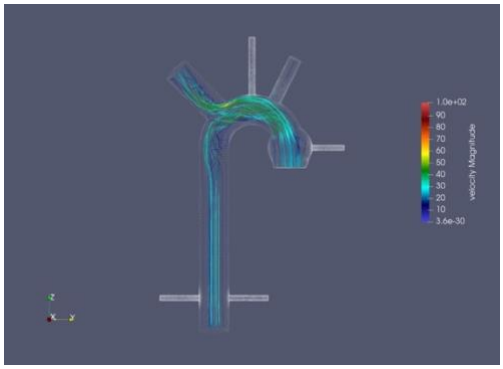

Figure 22: Vorticity: Axial-Flow LVAD on Ascending Aorta with Low LVAD Output

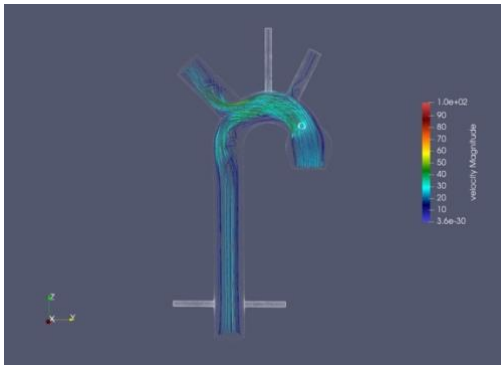

Figure 23: Vorticity: Transversal-Flow LVAD on Ascending Aorta with Low LVAD Output

Figure 20 to 23 present the streamlines of the flow, from which we may visualize the turbulence in the aorta. In the control group, the flow is mainly laminar with little to no turbulence. On the contrary, in the geometries with LVAD, even though laminar flow is still dominant, we found that the vorticity becomes more pronounced in the junction between descending aorta and aortic arch. Hence, to investigate this observed turbulence further, we focused the camera specifically onto the aortic arch.

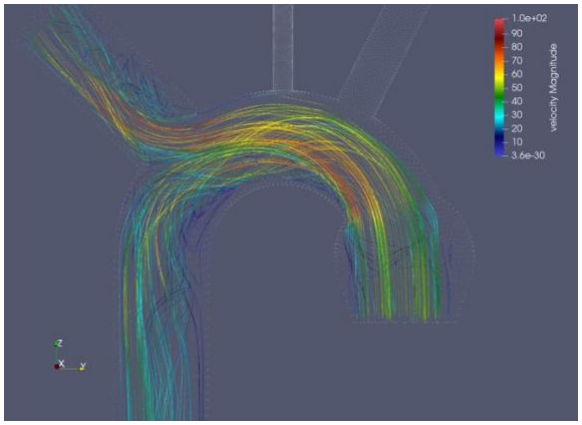

Figure 24: Detailed Vorticity: Control Group

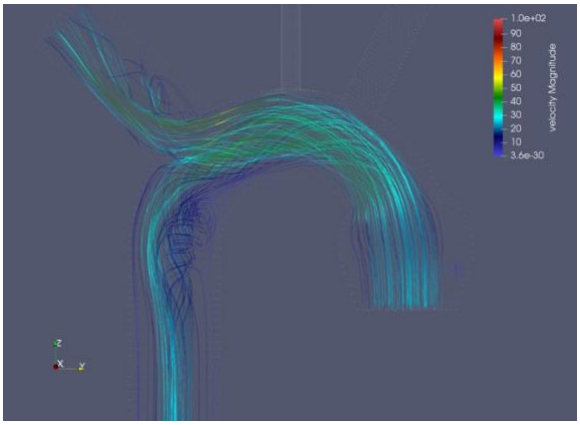

Figure 25: Detailed Vorticity: Axial-Flow LVAD on Descending Aorta with Low LVAD Output

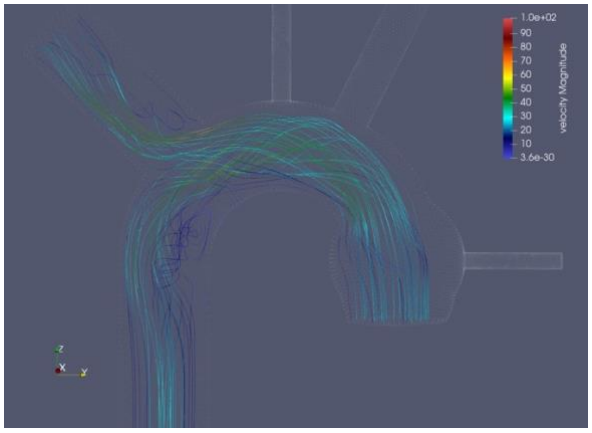

Figure 26: Detailed Vorticity: Axial-Flow LVAD on Ascending Aorta with Low LVAD Output

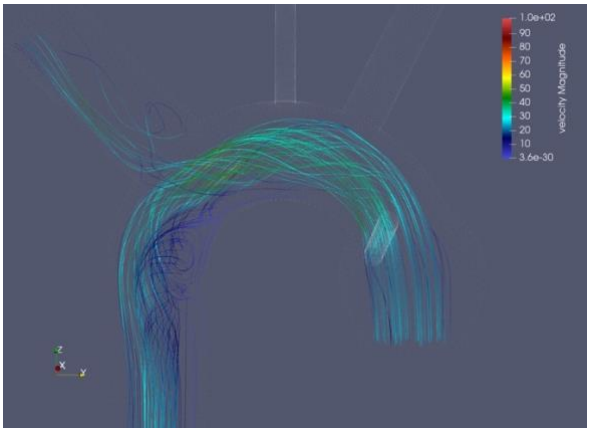

Figure 27: Detailed Vorticity: Transversal-Flow LVAD on Ascending Aorta with Low LVAD Output

Figure 24 to 27 are detailed vorticities on aortic arch. They suggest that, indeed, inside the aorta with LVAD, turbulent flow becomes more prominent compared to the control group. However, another observation that is worth to mention is the velocity magnitude where the turbulence takes place. The turbulent velocities are minimal and very close to 0, which suggests that their impact to the aortic wall may not be significant. Therefore, if a similar flow situation occurred in a natural aorta with LVAD, the impact of vorticity to aortic wall can be negligible.

5.2: High LVAD Output (70%)

LVADs are an promising option for end-stage heart failure patients. However, uncertainty remains regarding whether to adopt this approach. There are researches suggesting that if its utility is more than 70%, in another word due to congestive heart failure, left ventricle could only supply less than 30% of blood compared to premorbid heart, the implantation of LVAD should be considered. The high LVAD output (70% blood supply through LVAD) matches this condition.

5.2.1: Pressure

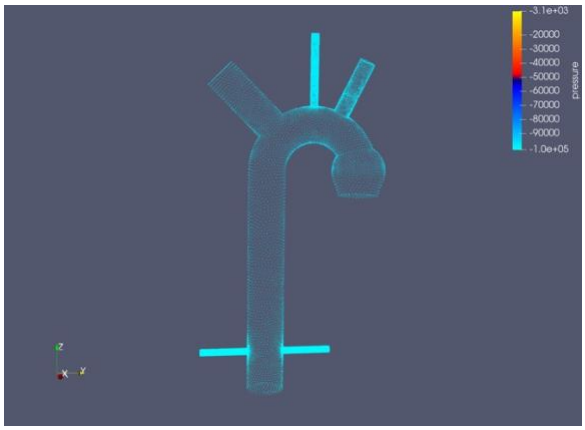

Figure 28: Pressure: Control Group

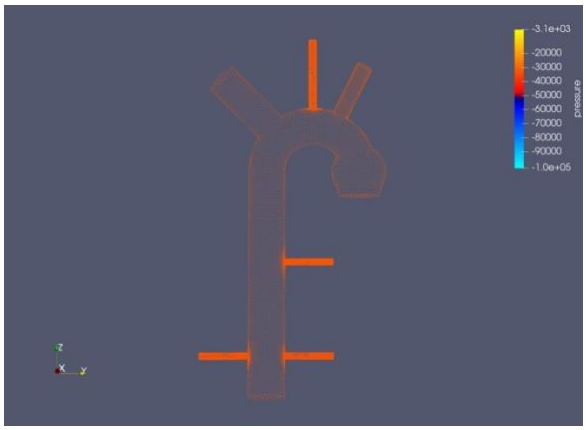

Figure 29: Pressure: Axial-Flow LVAD on Descending Aorta with High LVAD Output

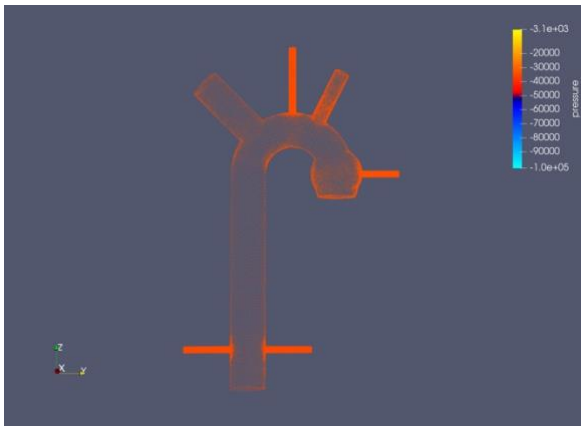

Figure 30: Pressure: Axial-Flow LVAD on Ascending Aorta with High LVAD Output

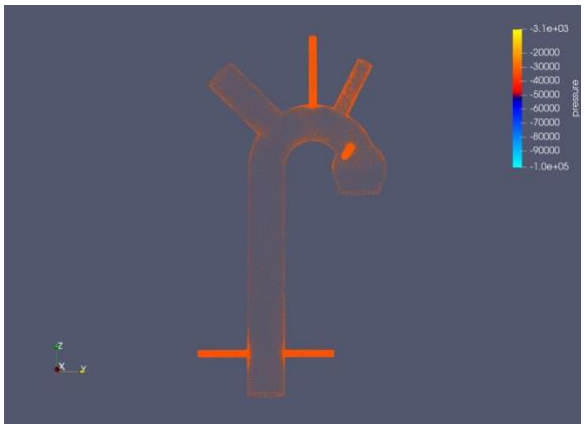

Figure 31: Pressure: Transversal-Flow LVAD on Ascending Aorta with High LVAD Output

Compared to the systolic aortic pressures in low LVAD output condition, the aortic pressure conditions associated with high LVAD output are further compromised. However, it seems that the pressure on aortic wall is still independent of the location of anastomosis.

5.2.2: Velocity

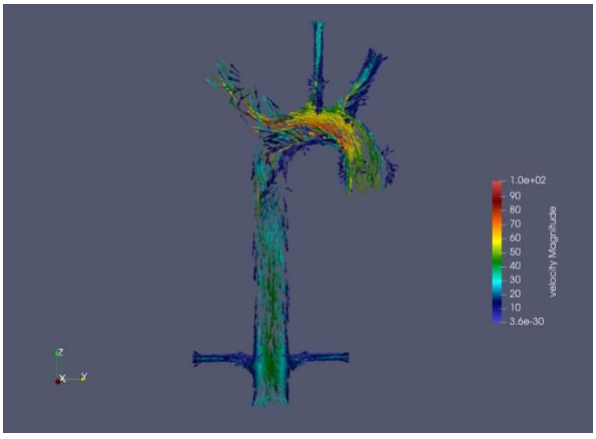

Figure 32: Velocity: Control Group

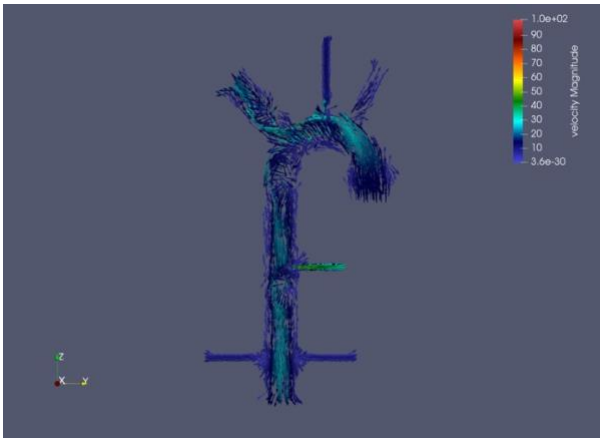

Figure 33: Velocity: Axial-Flow LVAD on Descending Aorta with High LVAD Output

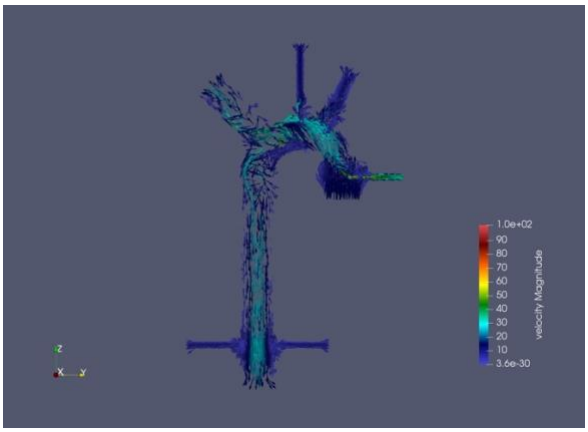

Figure 34: Velocity: Axial-Flow LVAD on Ascending Aorta with High LVAD Output

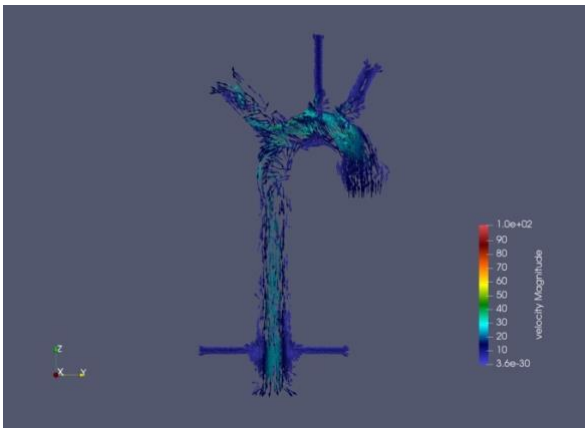

Figure 35: Velocity: Transversal-Flow LVAD on Ascending Aorta with High LVAD Output

Compared to the control group, we found, from figure 32 to 35, that the anastomosis under high LVAD output causes more disarrayed velocity vector field and this pattern was not observed under low LVAD output condition. In general, backflow or aortic valve regurgitation is undesirable in cardiovascular system, for it could potentially cause pumped blood to leak back into left ventricle. The leakage may prevent the heart from pumping blood efficiently and in turn could exacerbate the severity of heart failure. Since the backflow mainly concentrates in the aortic arch, we zoomed into this region and made following observations (Figure 36 to 39):

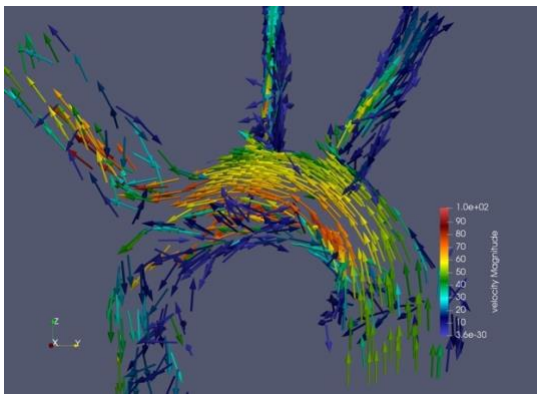

Figure 36: Detailed Velocity: Control Group

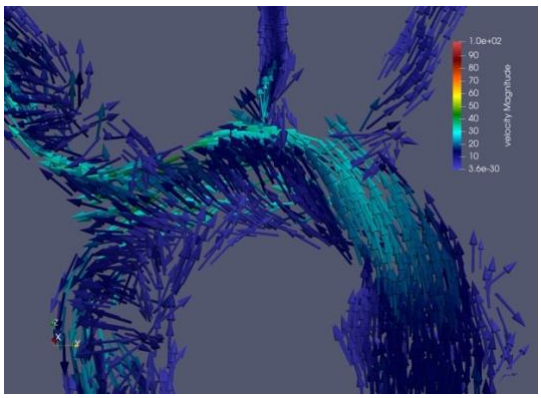

Figure 37:Detailed Velocity: Axial-Flow LVAD on Descending Aorta with High LVAD Output

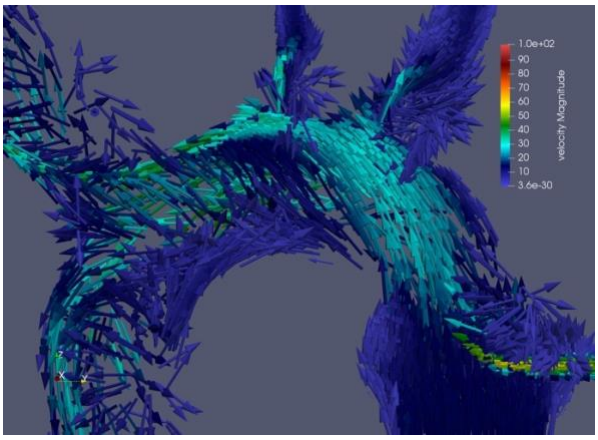

Figure 38: Detailed Velocity: Axial-Flow LVAD on Ascending Aorta with High LVAD Output

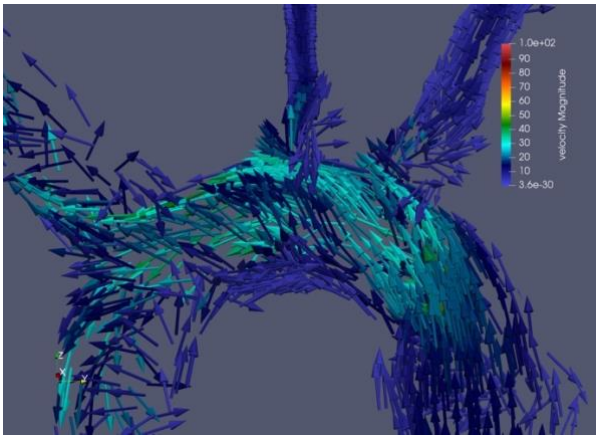

Figure 39: Detailed Velocity: Transversal-Flow LVAD on Ascending Aorta with High LVAD Output

In the control group, there is little to no backflow. Most of the flow originated from the aortic root adopts the pattern of laminar flow, going toward the outflow surfaces. However, under high LVAD output condition, all three models with various locations of anastomosis show some degrees of backflow with the axial-flow LVAD on ascending aorta being the most pronounced. In figure 38, the backflow region blockades the blood flow from the left ventricle, causing aortic regurgitation. The reverse flow may prevent the heart from efficiently pumping blood, which could potentially further exacerbate hear failure. On the other hand, compared to figure 38, figure 37 and 39 suggest that backflow is minimal in the aortic arch with axial-flow LVAD on descending aorta and with transversal-flow LVAD on ascending aorta. Hence, we investigated on the vorticity to determine which one of these two positions of anastomosis could resemble the control condition more closely.

5.2.3 Vorticity

Similar to low LVAD output condition, the vorticity associated with high LVAD output is the most pronounced in the junction between aortic arch and descending aorta.

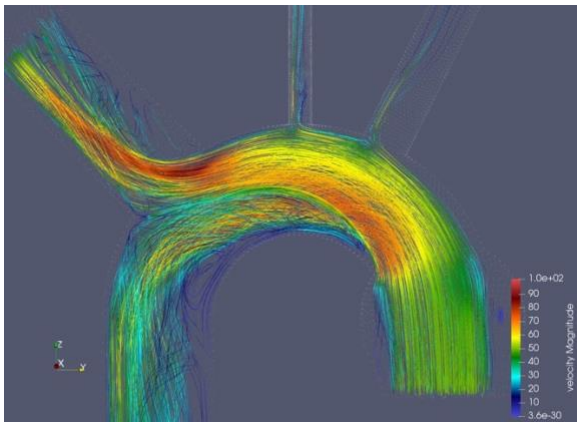

Figure 40: Axial Cross-sectional Vorticity: Control Group

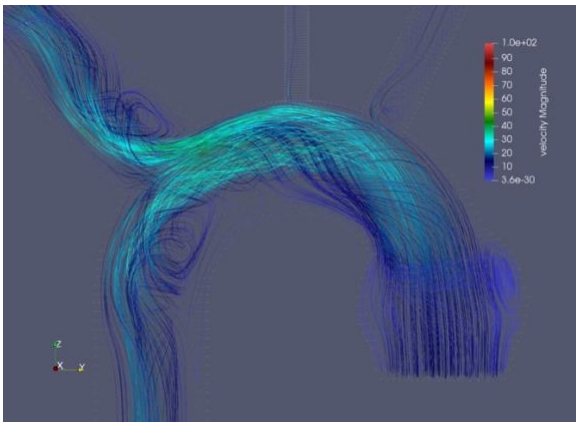

Figure 41: Axial Cross-sectional Vorticity: Axial-Flow LVAD on Descending Aorta with High LVAD Output

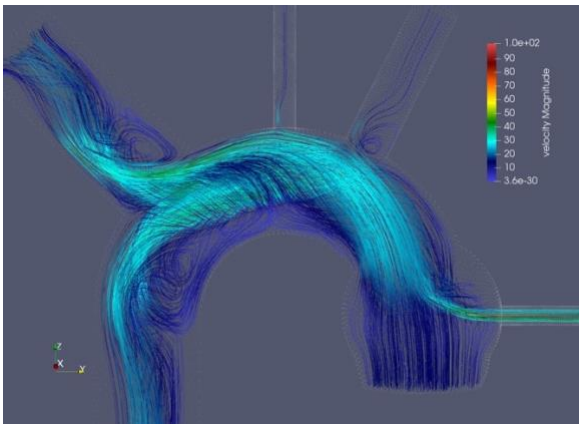

Figure 42: Axial Cross-sectional Vorticity : Axial-Flow LVAD on Ascending Aorta with High LVAD Output

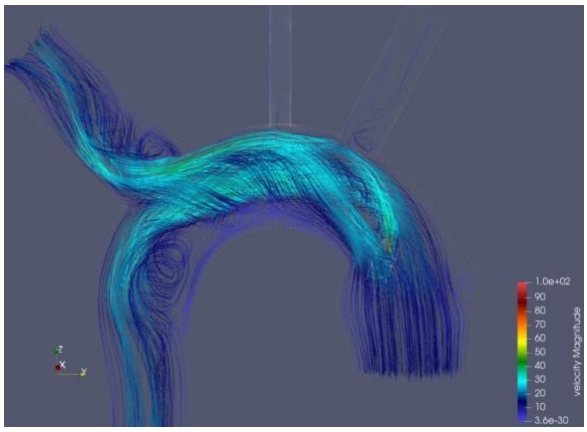

Figure 43: Axial Cross-sectional Vorticity: Transversal-Flow LVAD on Ascending Aorta with High LVAD Output

Figure 40 to 43 examine the vorticity in the axial cross-sectional area of aortic arch. In the control group, there is little to no turbulent flow. However, under high LVAD output, turbulent flow becomes much more evident in the aortic arch. Figure 42 and 43 exhibit the most pronounced vorticity in the aortic arch. On the contrary, albeit with some turbulence, figure 41 most closely preserves the integrity of hemodynamics of premorbid left ventricle. However, before we arrived to any conclusion, we also examined the vorticity in the transversal cross-sectional area of the aortic arch.

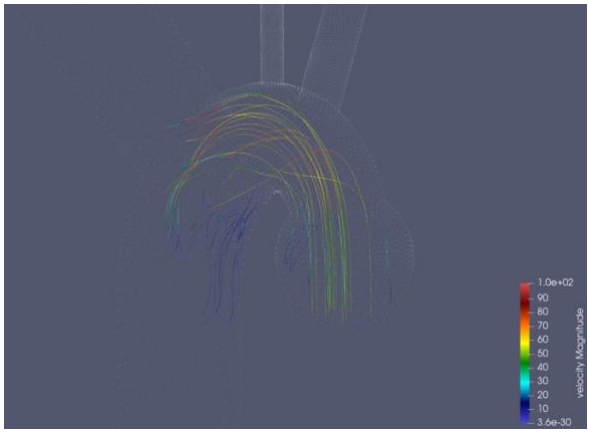

Figure 44: Transversal Cross-sectional Vorticity: Control Group

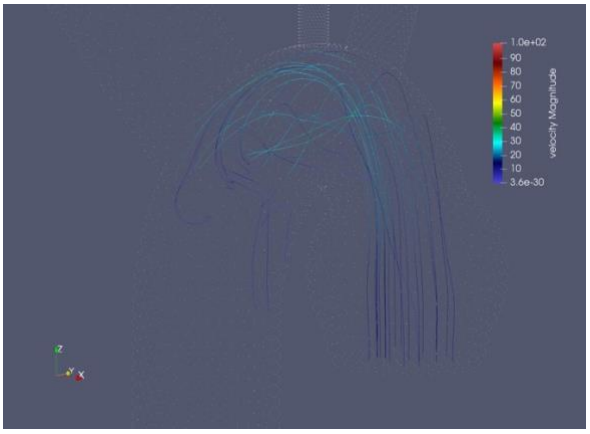

Figure 45: Transversal Cross-sectional Vorticity: Axial-Flow LVAD on Descending Aorta with High LVAD Output

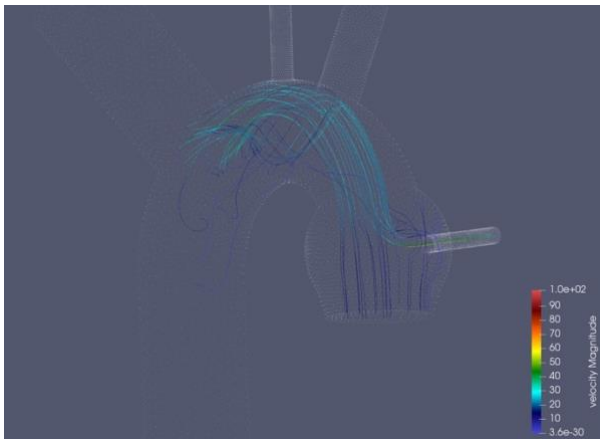

Figure 46: Transversal Cross-sectional Vorticity : Axial-Flow LVAD on Ascending Aorta with High LVAD Output

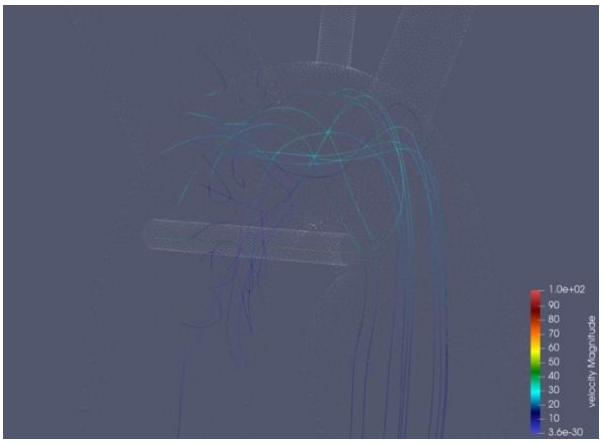

Figure 47: Transversal Cross-sectional Vorticity: Transversal-Flow LVAD on Ascending Aorta with High LVAD Output

The finding from figure 44 to 47 reaffirmed our conclusion. Figure 45 most closely resembles the laminar flow from the control group, whereas figure 46 and 47 exhibit stronger degree of turbulent flow. Therefore, under high LVAD output (70%), an axial anastomosis on descending aorta might be the most ideal solution for LVAD configuration.

5.3: 100% LVAD Output

When the aortic valve does not open or when heart failure causes 100% blockage of aortic root, LVAD is the only source to supply blood. Under this condition, 100% of the flow must occur through the LVAD over each cardiac cycle.

5.3.1: Systolic Pressure

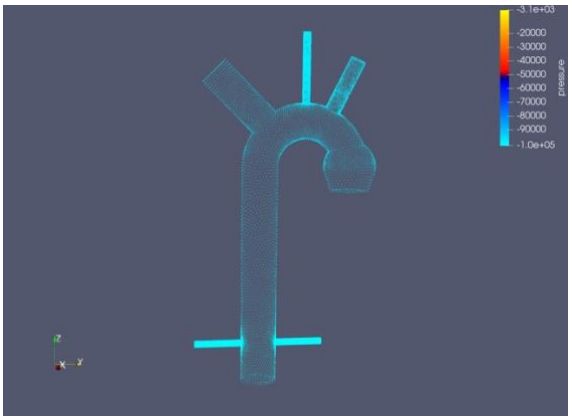

Figure 48: Pressure: Control Group

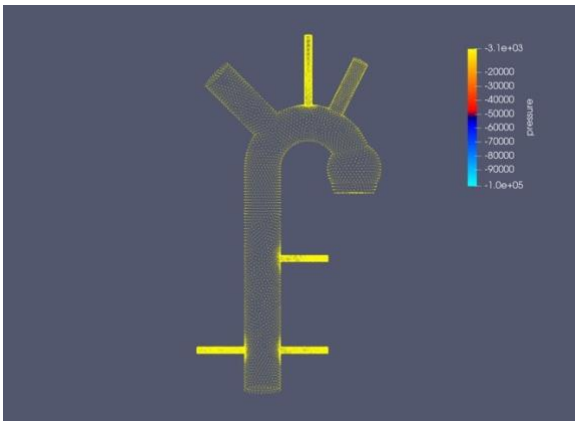

Figure 49: Pressure: Axial-Flow LVAD on Descending Aorta with 100% LVAD Output

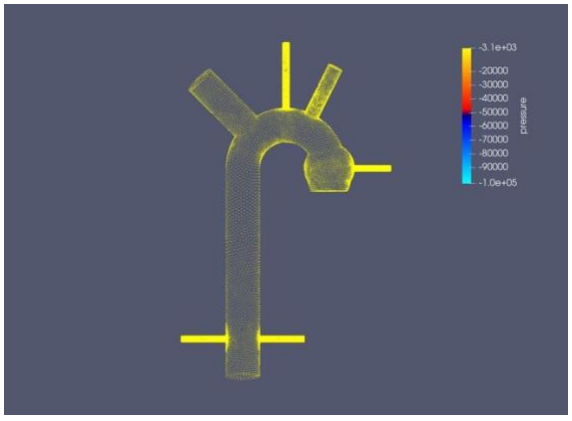

Figure 50: Pressure: Axial-Flow LVAD on Ascending Aorta with 100% LVAD Output

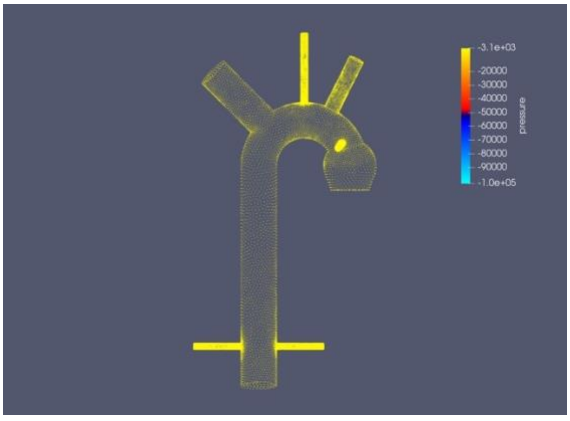

Figure 51: Pressure: Transversal-Flow LVAD on Ascending Aorta with 100% LVAD Output

Under 100% LVAD output condition, figure 49 to 51 suggest that the pressure on the aortic wall keeps decreasing as the LVAD output increases. The value of the pressure has no significant meaning but it reveals a trend of the pressure with respect to LVAD output. Again, the pressure on aortic wall is independent to the locations of anastomosis.

5.3.2: Velocity of Aortic Blood Flow

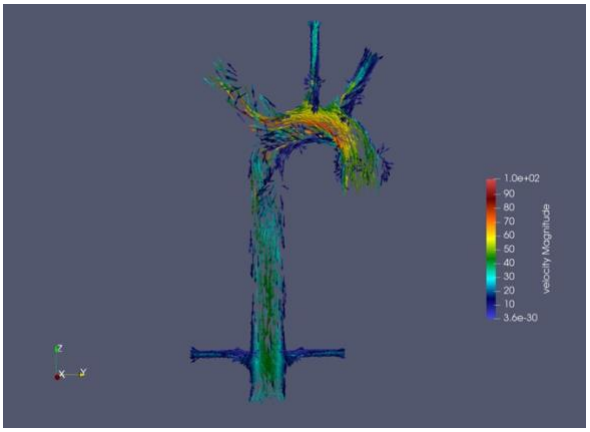

Figure 52: Velocity: Control Group

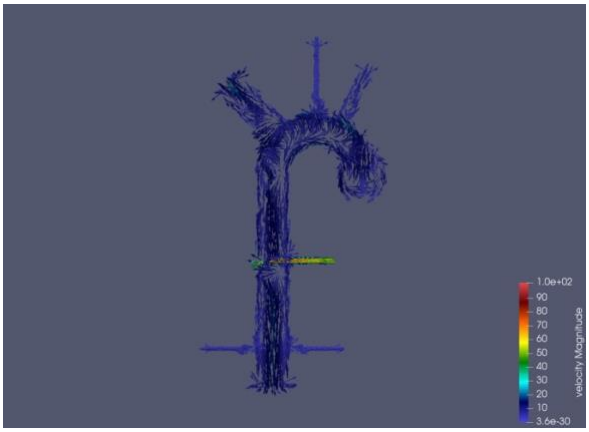

Figure 53: Velocity: Axial-Flow LVAD on Descending Aorta with 100% LVAD Output

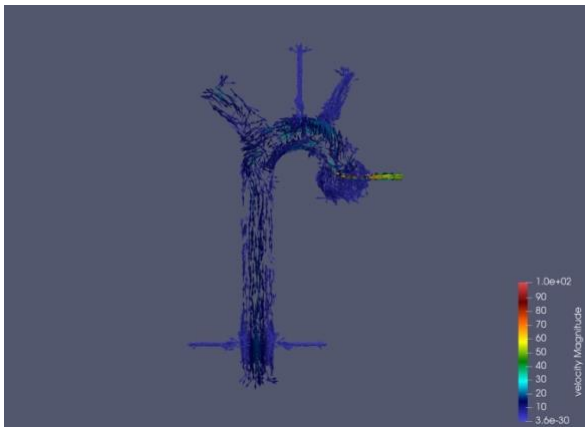

Figure 54: Velocity: Axial-Flow LVAD on Ascending Aorta with 100% LVAD Output

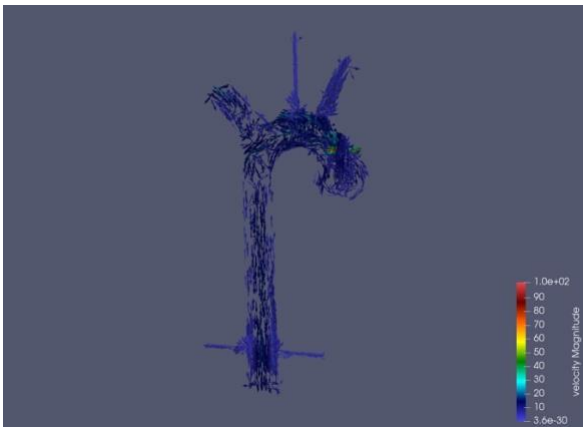

Figure 55: Velocity: Transversal-Flow LVAD on Ascending Aorta with 100% LVAD Output

100% LVAD output is an extreme case. It doesn't happen as often as the previous two cases, but it is worth to examine what approaches physicians should adopt if the left ventricular valve is completely closed. We prescribed 100% blood flow through LVAD. As figure 53 suggests, with a descending aortic anastomosis, the aortic root has a region of flow that is nearly stagnant. In contrast, as figure 54 and 55 suggest, with use of an ascending aortic out-flow graft anastomosis, a small degree of recirculatory flow may prevent complete stagnation at the aortic root. With the descending aortic anastomosis, no such recirculation could take place; instead, flow is static. Hence, axial-flow LVAD on descending aorta may lead to catastrophic consequence in this scenario. To compare the merit of the other two locations of anastomosis, we looked further into their vorticity conditions in the aortic arch.

5.3.3: Vorticity

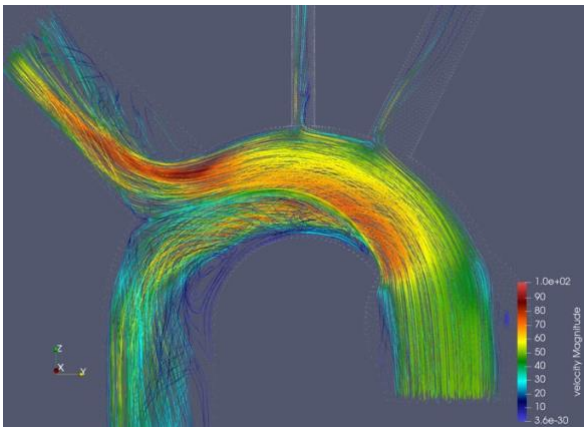

Figure 56: Axial Cross-sectional Vorticity: Control Group

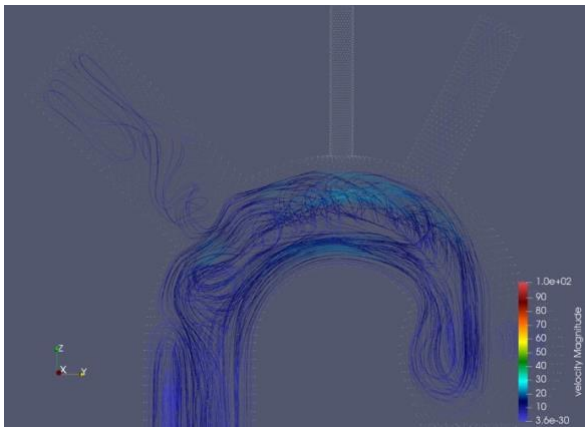

Figure 57: Axial Cross-sectional Vorticity: Axial-Flow LVAD on Descending Aorta with 100% LVAD Output

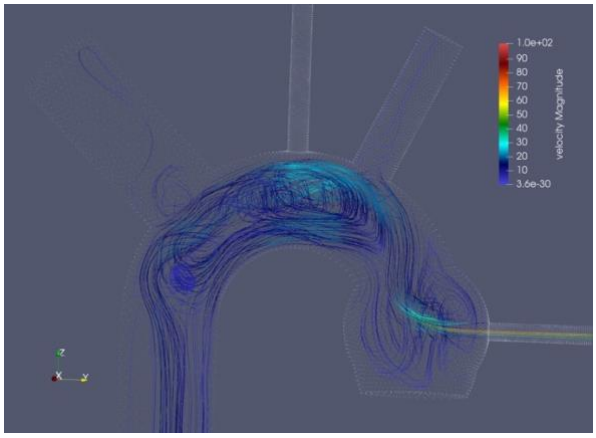

Figure 58: Axial Cross-sectional Vorticity : Axial-Flow LVAD on Ascending Aorta with 100% LVAD Output

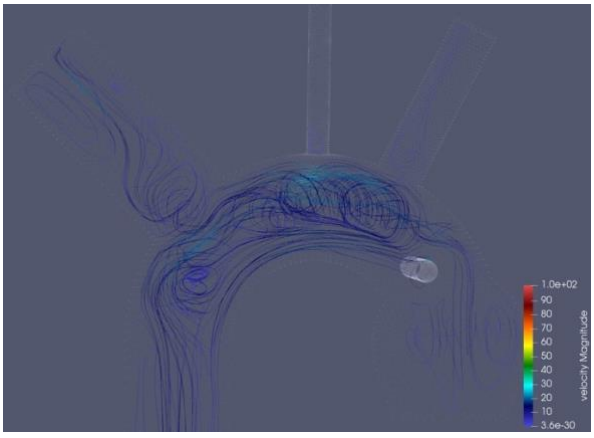

Figure 59: Axial Cross-sectional Vorticity: Transversal-Flow LVAD on Ascending Aorta with 100% LVAD Output

Compared to the control group, all aortic geometries with LVAD exhibit high vorticity in aortic arch. This implies that under 100% LVAD output, the flow is highly turbulent and could potentially lead to postsurgical intimal hyperplasia, which refers to proliferation and migration of vascular smooth muscle cells after surgery, resulting in the thickening of arterial walls. Given that the aortic valve is already completely shut due to heart failure, the development of postsurgical intimal hyperplasia could be lethal. Hence, to find the optimal location for anastomosis, we were

looking for the model that exhibit least vorticity or turbulent flow. In figure 59, transversal-flow LVAD on ascending aorta was configured and the vorticity it introduces into the aorta arch is minimal compared to the other two geometries. Therefore, under the condition of 100% LVAD output, we concluded that LVAD configuration on transversal surface of the ascending aorta may provide the most promising post-operational consequence.

6: Discussion

Aorta anastomosis is modeled with various positions of LVAD configuration. Two hundred simulations were performed overall to compare the effect of anastomosis locations on the altered systolic hemodynamics in the aorta. The altered systolic pressure, velocity and vorticity are examined individually under various LVAD output conditions and various locations of anastomosis.

Our simulations are instructive but the calculations are idealized in several respects. For who wishes to make quantitative predications on the basis of these simulations, the following limitations should be taken into consideration. The most serious limitation is the highly idealized nature of the aortic geometries. In this research, the geometries are idealized as a combination of cylinder, sphere and torus. However, in real physiological condition, shape and length of the aorta, LVAD outlet graft and anastomosis region would change due to time-dependent wall pressure and vascular muscle contractions. Correspondingly, hemodynamics would change too. The second limitation of the models is the simple treatment of the inflow and outflow boundaries. The third limitation of the model is the approximate evaluation of the vorticity. The vorticity in this research is determined through visualization of the blood flow through aorta. Moreover, the volumetric flow rate of the LVAD is not exactly pulsatile, as assumed here, but fluctuates with changing pressures in the aorta. All of these limitations will be considered in future simulation for a more accurate prediction of the altered hemodynamics. Nonetheless, the current simplified model of aortic flow remains unaffected by the previously mentioned error sources and can show qualitative hemodynamic differences resulted from various LVAD Output and the locations of LVAD configuration. Through analyzing the altered hemodynamics, this research also suggests the

optimal location to configure LVAD in surgical planning corresponding to various degrees of blockage of aortic valve.

The introduction of LVADs has significantly advanced the therapeutic options for patients with heart failure. Past research was directed to optimize their use to prevent known complications such as aortic valve cusp fusion and thrombosis in the aorta. Because LVAD provides a different path from left ventricle to aorta, it can make an impact on the vascular hemodynamics. This change may affect both the microvasculature and the microvasculature. The classic implantation configuration for LVAD is to draw blood from apex of the left ventricle and axially pumps it into the descending thoracic aorta or ascending aorta. In this research, we also ventured another possibility of LVAD implantation, which is to configure the LVAD through Transversal direction onto the ascending aorta. Few researchers have examined the impact of LVAD with this method of configuration.

To predict what alterations will be likely to occur, we must view the heart and aorta as a complex engineering system and only by adopting this perspective, could we apply the principles of fluid engineering. The model was driven by measured cardiac profiles and boundary conditions were formulated by considering pressure, resistance and stream diffusion condition. The model should be viewed as a computational analog to the real human aorta.

The simulations indicate that the location of the anastomosis has important qualitative effects on flow in the ascending aorta, aortic arch and descending aorta. Furthermore, they also suggest that with various extent of blockage of aortic valve, different locations of anastomosis should be adopted to optimize its benefit and to minimize the possibilities of potential postsurgical

complications. LVAD could be implanted, as discussed earlier, through the axial or Transversal direction on the ascending aorta or through the axial direction on the descending aorta.

When left ventricle is compromised due to heart failure and is only able to supply 50% of the blood flow toward the aorta, a physician would probably not recommend the approach of LVAD. This is not only because, for condition as such, the left ventricle itself is still sufficient to supply blood for daily activity, but also because the risks and potential complications associated with open heart surgery may outweigh its total benefit. Hence, medication and non-invasive procedures are more likely to be prescribed by a physician for the benefits of his or her patient's overall well-being and life-expectancy. However, in this scenario, if a physician chooses to adopt LVAD to compensate for the insufficient blood flow toward aorta, our simulations under low LVAD output condition (50%) suggest that its configuration location makes no significant impact on the hemodynamics of the aorta. The altered systolic pressure and blood velocity resemble closely to those of the premorbid heart and little to no vorticity and reverse flow could be visualized in the simulation results.

The decision of whether or not adopting the approach of LVAD may be rooted on the clinical experience of different physicians. A generally adopted criteria for considering LVAD is when the heart failure results in the left ventricle failing to supply more than 70% of the blood to the rest of the body. The condition as such is called end-stage congestive heart failure and the introducing of LVAD could be expected to improve a patient's survival and quality of life. For patients with end-stage congestive heart failure, LVAD can restore compromised total blood flow from left ventricle toward aorta back to its premorbid level. However, its side effect is also prominent; it can significantly disturb hemodynamics in the aorta. Our simulations in high LVAD output condition (70%) indicate that compared to a healthy individual whose blood flow in aorta

is mainly laminar, LVAD configuration could result in vorticity and reverse flow, which could be detrimental to the aortic wall and cause flow stagnation in aorta. The former is conducive for the development of aneurysm and the latter could potentially cause thrombosis. Therefore, we were looking into the LVAD configuration location that minimizes vorticity and reverse flow in aortic wall. As introduced earlier, the axial-flow LVAD on descending aorta could accomplish both. Therefore, outflow-graft anastomosis to the descending thoracic aorta is the optimal solution for high LVAD output condition (70%).

The most extreme case of heart failure is the complete closure of the aortic valve so that all of the output occurs through the LVAD. Heart failure at this stage is rare and lethal. However, investigation on this scenario could have significant implications on the choice of LVAD implantation location for heart failure with higher severity (70% or greater blockage of left ventricle). Under this condition, no blood flow could pass through the aortic root and LVAD is responsible for 100% blood supply. Our simulations under 100% LVAD output condition suggest that the blood flow in the aortic arch is highly turbulent with pronounced vorticity. Outflow-graft anastomosis to the descending aorta is no longer the optimal solution due to the accumulation of blood in the aortic root with little to no recirculation. This flow stagnation could further exacerbate the physiological condition of the patient at this stage of heart failure. On the contrary, with an ascending aortic anastomosis, a small degree of recirculatory flow in the aortic root may prevent complete stagnation. Moreover, our vorticity simulation with respect to the two ascending aortic LVAD indicate that turbulent flow in the aortic arch with transversal-flow LVAD is minimal,

which suggests that transversal-flow LVAD on ascending aorta is the optimal solution for heart failure with 100% blockage of the aortic valve.

In conclusion, the optimal location to configure LVAD on the aorta varies with respect to different severity of heart failure. Our simulations suggest that for 50% blockage of aortic root due to heart failure, if LVAD has to be implemented, all three locations may provide similar results with little to no difference. With around 70% blockage of aortic root, axial-flow LVAD on descending aorta may result in the most optimal post-operational consequence. With 100% blockage of aortic root or complete closure of aortic valve, transversal-flow LVAD on ascending aorta can be a promising solution. Unfortunately, there is no single solution for all cases.

Through clinical observation and computer modeling, we have begun to understand the complex physiology imparted by LVADs. In the future, we can look into the effect of various diameters of LVAD outlet graft and anastomosis angles on aortic hemodynamics. Similar researches have been conducted on two-dimensional geometric models, but the results will significantly differ in 3-dimensional space. I believe as we achieve greater understanding of implantation options and subsequent alterations of hemodynamics, it should be possible to tailor the best approach to each patient.

References

1. Kar, Biswajit et al. “The effect of LVAD aortic outflow-graft placement on hemodynamics and flow: Implantation technique and computer flow modeling.” *Texas Heart Institute journal* vol. 32,3 (2005): 294-8.
2. Inci, Gizem, and Esra Sorgüven. “Effect of LVAD Outlet Graft Anastomosis Angle on the Aortic Valve, Wall, and Flow.” *ASAIO Journal*, vol. 58, no. 4, 2012, pp. 373–381., doi:10.1097/mat.0b013e3182578b6a.
3. “Anatomy.” *AORTIC REFERENCE CENTER*, www.aortarepair.com/anatomy.html.
4. “Turbulent Flow.” *Image for Cardiovascular Physiology Concepts, Richard E Klabunde PhD*, www.cvphysiology.com/Hemodynamics/H007.
5. Delgado, Diego H., et al. “The Dilemma of a Left Ventricular Assist Device Explantation: A Decision Analysis.” *Canadian Journal of Cardiology*, vol. 23, no. 8, 2007, pp. 657–661., doi:10.1016/s0828-282x(07)70228-3.
6. Formaggia, Luca, et al. *Cardiovascular Mathematics*. Springer Milan, 2009.
7. Quarteroni, Alfio, et al. “Computational Vascular Fluid Dynamics: Problems, Models and Methods.” *Computing and Visualization in Science*, vol. 2, no. 4, 2000, pp. 163–197., doi:10.1007/s007910050039.
8. “Anatomy.” *AORTIC REFERENCE CENTER*, www.aortarepair.com/anatomy.html.